Research Square

Preprints are preliminary reports that have not undergone peer review.
They should not be considered conclusive, used to inform clinical practice,
or referenced by the media as validated information.

Single-Neuron Network Topology Governs Neural Computation and Learning in Primate Cortex

Yang Zhou

yangzhou1@pku.edu.cn

Peking University https://orcid.org/0000-0002-4517-1052

Zhuangyi Jiang

Peking University

Ziang Liu

Peking University

Li Shi

Peking University

Fang Fang

Peking University https://orcid.org/0000-0002-7718-2354

Shiming Tang

Peking University School of Life Sciences and Peking-Tsinghua Center for Life Sciences
https://orcid.org/0000-0003-0294-3259

Article

Keywords:

Posted Date: October 3rd, 2025

DOI: https://doi.org/10.21203/rs.3.rs-7541600/v1

License: This work is licensed under a Creative Commons Attribution 4.0 International License.
Read Full License

Additional Declarations: There is **NO** Competing Interest.

Version of Record: A version of this preprint was published at Nature Communications on April 30th, 2026. See the published version at https://doi.org/10.1038/s41467-026-72510-9.

Title: Single-Neuron Network Topology Governs Neural Computation and Learning in Primate Cortex

Authors: Zhuangyi Jiang[1#], Ziang Liu[1#], Li Shi[1], Fang Fang[1,2,3,5], Shiming Tang[3,4] & Yang Zhou[1,2,3,5*]

Affiliations:

[1] Peking-Tsinghua Center for Life Sciences, Peking University, Beijing, 100871, China

[2] School of Psychological and Cognitive Sciences, Peking University, Beijing, 100871, China

[3] PKU-IDG/McGovern Institute for Brain Research, Peking University, Beijing, 100871, China

[4] School of Life Sciences, Peking University, Beijing, 100871, China

[5] Beijing Key Laboratory of Behavior and Mental Health, Beijing, 100871, China

#: Those authors contributed equally.

* Corresponding author. yangzhou1@pku.edu.cn;

Abstract:

Neural networks underlie complex brain information processing, yet the role of their single-neuron topology in governing computation and behavior remains unclear, particularly regarding how it shapes individual neuron function and activity evolution during learning. Using two-photon calcium imaging, we tracked functional connectivity in thousands of posterior parietal cortex neurons as monkeys learned sensorimotor associations across days. We identified small-world networks with densely connected hub neurons that dominated encoding key task variables, driving local dynamics and neural encoding evolution during the monkeys' task performance and learning. Dynamic transitions in hub/non-hub status captured how inter-neuronal interactions shaped neuronal encoding evolution during association formation. Modular structures supported specialized neuron ensembles, enabling segregated representations and interactions within local networks. Importantly, small-world network properties predicted behavioral performance, with global information processing efficiency increasing as learning progressed. These findings reveal how single-neuron-resolution brain networks, through small-world organization, orchestrates both global and modular neural computations to mediate behavior and shape learning.

Main Text:

Neurons form complex networks in the brain that underlie various processes(*1-7*). Understanding these structural and functional networks at multiple scales is essential for elucidating how neural circuits contribute to overall brain activity and behavior(*8-12*). Previous studies using diverse research tools, such as magnetic resonance imaging (MRI), electrophysiological recordings, and neuronal tracing, have provided rich insights into both structural and functional neural networks, particularly at macroscopic scale(*13-22*). Quantitative analyses based on graph theory have illuminated the features of these complex brain networks(*1, 8, 23, 24*). However, much less is known about neural networks at single-neuron resolution in awake, behaving brain, primarily due to the technical challenges of mapping precise structural or functional connectivity among many neurons in behaving animals.

Network topology—defined by connectivity patterns and node positioning—systematically shapes the functional roles of its elements(*9, 25*). For instance, structural properties like degree distribution and modularity directly influence node dynamics(*25*), centrality measures (e.g., betweenness) predict functional importance in information flow or resource allocation(*26*), and highly connected 'hub nodes' are often functionally critical(*27*). However, how the functioning of individual neurons depends on their topology position in the neuron network remains largely unexplored. Moreover, learning is a dynamic process that fundamentally alters the structure and function of neuron networks(*28-33*). During learning, specific patterns of neuronal activity lead to the remodeling of neural connections, enhancing the efficiency of information processing within these networks(*31, 34*). Conversely, whether and how the network topology shapes the evolution of neuronal activity during learning remains unclear.

Small-world network topology, characterized by highly connected hubs and modularity, has been widely observed in both structural and functional brain networks(*1, 2, 5, 8, 14, 16, 17, 20, 22, 35-38*). This topology is hypothesized to be an efficient solution for achieving both global integration and functional segregation(*1, 5, 8, 39, 40*). Yet, the mechanisms by which the small-world topology of brain networks at single-neuron resolution optimizes neural processing to generate behavior and shape learning remain largely unknown, largely due to the lack of investigation into the topology of neuron networks during animals' task performance and learning. We hypothesize that highly connected hub neurons and the modular topology in small-world neuron networks play critical roles in global and modular neural processing, respectively. Specifically, hub neurons may dominate neural computations, such as neural encoding of behavioral variables and driving population activity dynamics, while modular connectivity could facilitate the formation of functionally specialized groups for segregated computations. We further propose that network topology coevolves with learning behavior, constraining the evolution of neural encodings of individual neurons and their mutual influences during learning.

PPC functional neuron network exhibited small-world topology

We directly tested these hypotheses by examining the functional network of hundreds of neurons simultaneously recorded from area 7a of the PPC in behaving monkeys, a region previously identified as a key hub for saccade planning and decision-making(*41-51*). We trained two monkeys to perform an image-saccade association learning task (**fig. S1**), where they had to choose one of

two saccade targets based on a presented visual image. The monkeys learned the associations between specific visual images and corresponding saccade directions through trial outcomes—receiving a juice reward for correct choices and a short time-out punishment for incorrect ones (see Methods). Once the monkeys fully mastered two image-saccade associations (accuracy 0.89±0.05, mean ± STD), they were required to learn a pair of novel associations in subsequent days. We employed two-photon calcium imaging to simultaneously record the activity of hundreds of neurons over multiple days. We tracked the activity of the same population of neurons across a whole learning course, starting from the first day when monkey was tested with a pair of familiar associations to the day they mastered a new pair of associations for each recorded field of view (FOV, subregion). We successively finished recording from 12 FOVs and identified a total of 8537 single neurons with a good signal-to-noise ratio in two monkeys. Additionally, our previous study demonstrated that primate area 7a is involved in associative learning and that functional connectivity among 7a neurons may constrain the evolution of neuronal encoding across learning days(*52*). This dataset offers a unique opportunity to explore how network topology at single-neuron resolution optimizes neural processing to generate behavior and shape learning.

To construct the functional neuron network, we calculated the partial noise correlation between each pair of simultaneously recorded neurons within each recording session, using these correlation values as the connection weights between neurons. We then applied a threshold to these connection weights to create a connection (adjacency) matrix representing the neuron network (**Fig. 1A**, see Methods). Partial noise correlation has been demonstrated to be an effective measure of the functional connectivity in neuron networks at the scale of a few hundred neurons(*53*). While it does not necessarily represent monosynaptic connection, it reflects the influence of one neuron on another, significantly reducing the impact of common input and task-related modulation. On average, these PPC neuron networks consist of approximately 144 neurons (144±22), and the sparsity of their connection matrix was 0.048±0.013. Notably, connection weights within the PPC neuron networks were stronger between neurons that exhibited similar encoding selectivity during monkeys' task performance, compared to neurons with opposite encoding preferences (**Fig. 1, B, C**). Additionally, the connection weights did not significantly correlate with the spatial distance between neurons within most FOVs (**fig. S2**).

We next applied graph theoretical analysis to the PPC neuron networks, revealing significant deviations from random network properties. All observed networks demonstrated substantially greater standard deviations in average connection degrees compared to matched random networks (Poisson and Binomial distributions with equivalent connection degrees; **Fig. 1D**). The distribution of connection degrees consistently showed heavy-tailed characteristics (**Fig. 1E**). Notably, all the PPC neuron networks exhibited small-world properties (**Fig. 1F**): clustering coefficients, quantifying the degree of local clustering, were approximately six-fold greater than those of random networks, while the characteristic short-path lengths were comparable to those of random networks. This combination resulted in small-worldness values several times greater than those of random networks.

Interestingly, within each the network, we identified a subset of neurons which are densely connected with each other and with other neurons, while the remaining neurons were more sparsely connected (**Fig. 1G** and **fig. S3, A, B**). By maximizing the coreness statistic—ensuring maximal

hub-to-hub and minimal non-hub-to-non-hub connections (see Methods)—we classified these two subsets as hub and non-hub neurons, which were present in roughly equal numbers within each network. The hub and non-hub topology of network organization was further supported by calculating the $Q_{(core)}$ coefficient, which quantifies the goodness of fit for the core/periphery model to the network, for all (but one) the networks (**Fig. 1H**). Although hub and non-hub neurons were spatially overlapped in the cortex (**fig. S4**), hub neurons exhibited significantly greater connection strength and degree compared to non-hub neurons (**Fig. 1, I, J,** $P_{(strength)}$ = 1. 6e-53, t(58) = 59.1, $P_{(degree)}$ =1.2e-46 , t(58) = 44.7, paired t-test). Additionally, connections between hub neurons were more stable, gaining or losing connections less frequently across learning days compared to connections between hub and non-hub neurons or between non-hub neurons (**Fig. 1, K, L**). Interestingly, hub neurons exhibited greater fluorescence luminance and larger size on average than non-hub neurons (**fig. S5, A, B**), potentially indicating physiological difference between the two subsets. However, these differences in luminance and size did not substantially contribute to the neurons' hub and non-hub status (**fig. S5, C, D**).

Furthermore, modularity analysis revealed significant modular organization in all PPC neuron networks (**Fig. 1M**, example network), with modularity coefficients substantially exceeding those of random networks (**Fig. 1H,** P = 5.0e-34, t(58) = 26.4, t-test). On average, within-module connections showed significantly stronger weights and higher density, along with shorter path lengths, compared to between-module connections (**Fig. 1, N** to **P,** $P_{(weight)}$ = 1.1e-46, t(58) = 44.8, $P_{(density)}$ =1.6e-49 , t(58) =50.3 , $P_{(path\ length)}$ =3.0e-31, t(58) =-23.4 , paired t-test). Moreover, spatial clustering of neurons within modules was also evident (**fig. S6**). Together, these results demonstrate that the PPC neuronal network in behaving monkeys exhibits a classical small-world topology.

Hub neurons exhibited greater and more stable encodings on task variables

Considering the phenomenon where hub neurons exhibit higher connection degrees and strengths, we hypothesize that these neurons facilitate global information processing within local networks through two distinct mechanisms compared to non-hub neurons. First, hub neurons likely contribute more significantly to encoding information critical for mediating task performance. Second, they may play a dominant role in driving the activity dynamics within local network. To test these hypotheses, we initially examined how neurons encoded key task variables during the ISAL task, such as saccade direction and trial outcome, across each network. We found that the strength of encoding for both task variables positively correlated with the centrality of individual neurons (**fig. S7**), a fundamental measure of hubness. Consequently, hub neurons exhibited significantly stronger encoding of both saccade direction and trial outcome across most networks (**Fig. 2, A, B**: example neurons; **Fig. 2, C, D**: example session; **Fig. 2, E, F**: population). These results suggest that hub neurons might play a primary role in the neural representation of key task variables.

Previous studies have demonstrated that the neural encoding in PPC evolved across different time periods during learning(*52*). We therefore examined the stability of neuronal encodings at the population level across different time periods separately for both hub and non-hub neurons through two complementary approaches. First, we assessed correlations in the patterns of neuronal

selectivity for both saccade direction and trial outcome across different time periods within and between recording sessions (see Methods). We observed greater correlations among hub neurons compared to non-hub neurons in most networks, whether across different time periods within a single recording session or across successive learning days (**Fig. 2, G, H**). This indicates greater encoding stability in hub neurons during learning. Second, we evaluated the stability of population neural codes by measuring the alignment between neural subspaces of population activity across different time periods. Using an alignment index ranging from 0 (perfect orthogonality) to 1 (perfect alignment; see Methods), we found that hub neurons consistently showed significantly higher alignment indices than non-hub neurons, both within individual learning session and between successive learning days (**Fig. 2, I, J**), further confirming more stable neuronal encoding in hub neurons. Together, the stronger and more stable neuronal encodings indicate that hub neurons might play a primary role in encoding key task variables to mediate the neural computations within local network.

Hub neurons contributed more to the activity dynamics within network

Next, we tested the hypothesis that hub neurons dominate the activity dynamics within network during the monkeys' task performance and learning. Initially, we examined the effect of hub versus non-hub neurons on the population activity dynamics within network. We performed principal component analysis (PCA) to reduce the dimensionality of the population activity during monkeys' task performance and projected it onto the top 10 PCs that explained the majority of the variance in population activity (91.4%). This revealed that hub neurons contributed significantly more to the dynamics of the population activity compared to non-hub neurons, as reflected by their stronger weighting on these PCs (**Fig. 2K** and **fig. S8**).

We then measured how each neuron's current activity influenced the future activity of other neurons within the local network using a causality index, defined as the partial correlation between a neuron's activity in the current time period and the activity of other neurons in future time periods within the same task trial, conditioned on the current activity of these neurons (see Methods). This index quantifies directional influence strength, with higher absolute value indicating greater influence of a neuron's activity on the activity dynamics of other neurons over time. We computed the causality index across successive time frames for both hub and non-hub neurons. Across networks, hub neurons exhibited significantly higher outgoing causality (influencing other neurons) but lower incoming causality (being influenced) compared to non-hub neurons. (**Fig. 2, L, M** and **fig. S9, A** to **C**). These results suggest that, during the monkeys' task performance, hub neurons exerted a stronger influence on the activity dynamics of other neurons, while non-hub neurons were more susceptible to influence by other neurons.

Furthermore, we calculated the causality index using data from two successive learning days to assess the influence of hub and non-hub neurons on changes in neuronal encoding during learning. To achieve this, the causality index was computed based on neuronal selectivity to different task variables (see Methods). Specifically, we quantified how the activity of one neuron influences the evolution of neural encoding in another neuron from one learning day to the next, which we termed the 'exerted learning effect". Conversely, we assessed how the evolution of neural encoding in one neuron, from the previous learning day to the current day, is influenced by the activity of another

neuron from the previous day, referring to this as the 'received learning effect'. We found that hub neurons exhibited greater exerted learning effects and greater received learning effects compared to non-hub neurons, as reflected by higher absolute values of the causality index (**Fig. 2, N, O** and **fig. S9, D, E**). Notably, the greater received learning effect in hub neurons was observed only during successive learning days when the monkeys were learning the same associations, and was absent when they transitioned from familiar associations to new ones (**Fig. 2P**, $P_{(learning)}$ = 5.3e-05, t(34) = 4.6; $P_{(transition)}$ = 0.85, t(11) = 0.19, paired t-test). Additionally, hub neurons showed greater exerted learning effects when quantifying the influence of neuronal activity on activity evolution from the first to the second half of one learning day (**Fig. 2Q**, P = 2.8e-17, t(58) = 12.0, paired t-test). Together, these findings suggest that hub neurons play a dominant role in shaping the evolution of neuronal encoding within the local network during learning.

Transitions of neurons' hub/non-hub status across successive learning days

Interestingly, the network's hub/non-hub architecture exhibited dynamic reorganization during learning, with neurons transitioning between hub and non-hub status. Specifically, some neurons lost hub status (hub-losing neurons), while others gained it (hub-gaining neurons). Meanwhile, other subsets of neurons maintained their hub/non-hub status across successive learning days: stable hub neurons (consistently identified as hubs) and stable non-hub neurons (which retained their non-hub status). Consistent with these topological changes, hub-gaining neurons acquired more network connections than other neurons across successive learning days (**fig. S10A**), while hub-losing neurons lost network connections more frequently than both stable hub neurons and hub-gaining neurons (**fig. S10B**, $P_{(hub\text{-}losing\ vs.\ stable\ hub)}$ =2.3e-25, t(46) = -21.2, $P_{(hub\text{-}losing\ vs.\ hub\text{-}gaining)}$ =8.5e-23, t(46) = 18.4, paired t-test).

We then quantified topological differences between these neuron subsets using the diversity coefficient, which quantifies each neuron's inter-module connections relative to its within-module connections (see Methods). Hub neurons exhibited significantly higher average diversity coefficients than non-hub neurons (**Fig. 3A**, P = 2.3e-30, t(46) = 27.7, paired t-test), indicating that non-hub neurons were more likely to remain confined within a module, whereas hub neurons formed broader inter-module connections. Specifically, the diversity coefficient was significantly higher in stable hub neurons compared to hub-losing neurons (**Fig. 3B**, P = 6.5e-6, t(46) = 5.1, paired t-test), as well as in hub-gaining neurons compared to stable non-hub neurons (P =1.7e-6, t(46) = 5.5, paired t-test). Critically, hub-losing neurons exhibited reduced negative inter-module connections but maintained similar positive inter-module connections relative to stable hub neurons (**Fig. 3C** and **fig. S10, C, D**, $P_{(positive)}$ = 0.61, t(46) = 0.52, $P_{(negative)}$ = 1.6e-10, t(46) = 8.2, paired t-test). This resulted in hub-losing neurons exhibiting the strongest dominance of positive over negative inter-module connections among all neuron subsets (**Fig. 3D**). Similarly, hub-gaining neurons showed a greater dominance of positive over negative inter-module connections compared to stable non-hub neurons (P = 0.0011, t(46) = 3.5, paired t-test). These findings suggest that relative positive inter-module participation predicted hub/non-hub status transitions during learning.

Consistent with the dynamics of the hub/non-hub status across learning days, hub-losing neurons exhibited significantly weaker encoding of the task variables after the transitioned compared to the

preceding day (**Fig. 3, E, F**), whereas hub-gaining neurons exhibited significantly stronger task-related encoding following the transition (**Fig. 3, G, H**). Furthermore, Stable hub neurons displayed stronger connection weights and greater neuronal encoding of key task variables compared to hub-losing neurons (**fig. S10, E** to **G**). Similarly, hub-gaining neurons exhibited a trend toward stronger connection strengths and neural encoding than stable non-hub neurons (**fig. S10, H** to **J**). Additionally, stable hub neurons demonstrated greater encoding stability than other subsets of neurons (**fig. S10K**, p =4.2e-8, t(46) = 6.6, paired t-test).

Interestingly, neurons that transitioned between hub and non-hub statuses exhibited distinct patterns of influence on changes in neuronal encoding across successive learning days. Hub-losing neurons demonstrated greater exerted learning effects than other neurons, suggesting that those hub neurons that exert a stronger influence on others' activity are more likely to lose their hub status during learning (**Fig. 3I**, P =8.7e-7, t(140) = 5.1, paired t-test). Conversely, hub-gaining neurons exhibited greater received learning effects, indicating that non-hub neurons more influenced by others' activity are more likely to assume a hub role after learning (**Fig. 3J**, P =7.8e-8, t(140) = -5.7, paired t-test). Notably, hub-losing neurons exhibited greater exerted learning effects than stable hub neurons (P = 0.035, t(34) = 2.2, paired t-test) despite weaker neural encodings. Similarly, hub-gaining neurons received greater learning effects than stable non-hub neurons (P =0.041, t(34) = -2.1, paired t-test), despite stronger neuronal encodings. This suggests that neurons that switched between hub and non-hub statuses during successive learning days were more likely to exert a stronger influence on, or receive a greater influence from, other neurons' activity during learning.

Moreover, the greater exerted learning effect in hub-losing neurons and greater received learning effect in hub-gaining neurons was observed only during the learning days when the monkeys were learning the same associations, absent during the successive days when they transitioned from familiar to novel associations (**Fig. 3, K, L**). Together, these results suggest that the changing dynamics of neurons' hub/non-hub status across successive learning days were not random fluctuations, but were instead shaped by their inter-modular connectivity. Specifically, these status transitions closely linked to the neurons' differential influence on the evolution of neuronal encodings of other neurons, particularly during the acquisition of novel associations.

Modular computation within PPC neural network

We next investigated how the modular structure of the PPC neuron network facilitates modular neural computation. An intuitive expectation is that modular connectivity patterns form function specified groups within local networks, which enable functional segregation during neural computation. To test it, we quantified the similarity of neuronal encodings among individual neurons both within and across modules. We observed significantly higher signal correlation and noise correlation between neurons within the same module compared to those across different modules in most networks (**Fig. 4, A, B,** $P_{(signal)}$ =2.0e-22, t(58) =15.6, $P_{(noise)}$ = 1.6e-27, t(58) = 19.8, paired t-test). Neuronal representations of saccade direction and trial outcome were partially separated between different modules (**Fig. 4C**, P = 6.2e-10, t(58) = 7.4, paired t-test). Additionally, PPC neurons exhibited more consistent neuronal encodings on individual task variables within modules than across modules, with greater neural selectivity similarity observed for both saccade

direction and trial outcome (**Fig. 4, D, E,** $P_{(saccade)}$ = 4.9e-23, t(58) = 16.1, $P_{(outcome)}$ = 3.3e-21, t(58) = 14.7, paired t-test). Furthermore, changes in neuronal encodings were more similar between neurons within the same module compared to neurons from different modules, both within a single learning day and across successive learning days (**Fig. 4, F, G**, $P_{(within\ session)}$ = 2.5e-21, t(58) = 14.8, $P_{(across\ session)}$ = 1.9e-15, t(46) =11.7, paired t-test). These results indicate that neurons were functionally more similar within the same module than across modules.

Furthermore, we examined whether the modular connectivity constrained the activity dynamics of individual neurons during monkeys' task performance and learning. We predicted stronger mutual influence between neurons from the same module (within-module pair) than between neurons from different modules (across-module pair). Specifically, neurons may drive the activity of other neurons within the same module to be more similar to their own activity compared to neurons from different modules. To test this, we calculated the causality index separately for within-module and across-module pairs using condition-averaged activity across successive time frames within a task trial. We found a higher causality index for the within-module pair compared to the across-module pair in most networks (**Fig. 4H,** $P_{(+1f)}$ = 2.3e-25, t(58) = 18.0, $P_{(+2f)}$ = 3.4e-23, t(58) = 16.2, $P_{(+3f)}$ = 3.7e-20, t(58) = 13.9, paired t-test), suggesting that within-module pair had a stronger mutual influence on their activity dynamics during monkeys' task performance.

Additionally, we calculated causality index to quantify how neurons' activity influenced the changes in other neurons' encodings of task variables either from the first to the second halves of a single learning session or from the current to the next learning days. This also revealed greater causality indexes for the within-module pair compared to the across-module pair (**Fig. 4, I, J,** $P_{(within\ session)}$ = 2.2e-18, t(58) =12.7, $P_{(across\ session)}$ = 3.4e-11, t(46) =8.6, paired t-test), indicating that within-module pair had a greater mutual impact on the evolution of neuronal encoding during learning compared to across-module pair. These results collectively demonstrate that neurons within the same module were functionally more similar and exerted a stronger mutual influence on activity dynamics and neural encodings than those across modules during the monkeys' task performance and learning.

Network topology predicted the similarity of neuronal encodings and monkeys' behavioral performance during learning

To further investigate how small-world network topology influences the functional roles of PPC neurons and shapes activity evolution during learning, we tested whether the topological position of neurons could predict the similarity of their neural encodings during learning. Specifically, we employed a linear model incorporating parameters of network topology to predict the signal correlations between all pairs of recorded neurons for each PPC network (see Methods). This model primarily considers four topology parameters for each pair of neurons: the hub and non-hub status, the modular organization, the relative connection weight between them, and their topological overlap.

Our model significantly predicted the signal correlation between neurons within the PPC neuron network. On average, these four parameters explained more than 19% of the variance in signal correlation between all neurons, which was significantly greater than the shuffled control **(Fig.**

5A). For most networks, all four parameters contributed significantly to the model's performance **(fig. S11)**. Additionally, these four parameters also significantly predicted the similarity of neuronal encodings on the following learning days. These findings further underscore the role of network topology in governing neuronal functions.

Finally, we examined the relationship between network topology and the monkeys' daily behavioral performance during learning. Using a stepwise linear model with a set of PPC network topological parameters, we predicted the monkeys' daily performance and applied the Bayesian Information Criterion to identify the most relevant variables (see Methods). This revealed that the small-world topology of the PPC neuron network significantly predicted the monkeys' performance accuracy during associative learning, with the characteristic path length, modularity, and their interaction as the significant predictors (**Fig. 5B** and **fig. S12A**, $R^2 = 0.33$, $P<0.001$, permutation test). Specifically, as the monkeys' performance accuracy improved across learning days, the averaged short-path length of the network decreased, and network modularity became less pronounced (**table. S1**). This suggests that global information integration and communication within the local PPC neuron network became more efficient with learning.

To further investigate the relationship between PPC network topology and the monkeys' choice strategies during associative learning, we employed the dynamic PsyTrack model to fit the monkeys' daily choice accuracy(*54*) (see Methods). This resulted in two weights, $W_{stimulus}$ and W_{bias}, reflecting the influence of visual stimuli and internal bias on the monkeys' saccade choices, respectively. We modeled these weights independently using linear models incorporating PPC network topological features. This revealed that connection density, short-path length, and modularity coefficient were significant predictors of the monkeys' choice bias (**table. S1**, **Fig. 5C** and **fig. S12B**, $R^2 = 0.23$, $P=0.004$, permutation test). Specifically, the monkeys showed a greater saccade choice bias toward the contralateral target when connection density was higher, short-path length was smaller, and network modularity was more pronounced. In contrast, short-path length, modularity coefficient, and their interaction were strong predictors of correct choices based on stimuli (**table. S1**, **Fig. 5D** and **fig. S12C**, $R^2 = 0.37$, $P<0.001$, permutation test). Improved choice performance was associated with more efficient global integration (smaller short-path length) and less local computation (weaker modularity) within the local neuron network.

Discussion:

Together, we constructed the functional neuron network in the monkey PPC during long-term learning using partial noise correlation. We found that PPC neuron networks exhibited small-world properties, with network topology significantly shaping the functional roles and activity dynamics of individual neurons during the monkeys' task performance and learning. Specifically, the densely connected hub neurons played a primary role in representing key task variables and driving the activity dynamics to support global information processing, while the modular structure formed the basis of neuron ensembles, enabling modular information processing within the local network. Notably, the small-world network dynamics across learning days not only captured how inter-neuronal interactions shaped the evolution of neuronal encoding during novel association learning but also reflected the monkeys' behavioral performance and learning strategies, with global neural computation within local networks becoming increasingly efficient as learning advanced. These

results provide direct evidence in behaving animal showing how the topology organization of brain network at single-neuron resolution facilitates both global and modular information processing to mediate task performance and learning, establishing a mechanistic link between microscale network organization, neural computation, and behavior.

Small-world topology, well-documented across different brain networks (*1, 2, 5, 10, 12-17, 20-22, 35, 36, 38, 55-60*), is now demonstrated at the neuronal level through two-photon calcium imaging in behaving monkeys, supporting its role as a fundamental principle of brain organization. While previous work has established the benefits of small-world architecture for efficient information transfer, synchronization, and robustness with minimal wiring costs in various neural processes(*5, 39, 40*), our study reveals how this topology shapes both individual neuron functions and inter-neuron interactions. Specifically, we uncover mechanisms by which how hub-dominated global processing and module-specific segregation emerge as organizational principles that constrain neuronal encodings, regulate information flow, and govern local activity dynamics - providing a cellular-level explanation for how neural computations emerge to support behavior and learning.

Hub nodes represent fundamental network features that serve critical integrative functions. In macroscopic brain networks, hub areas form densely interconnected core circuit cross-liking all major functional subsystems(*12, 13, 58, 59*). At the cellular level, hub neurons - identified both in vitro and in the brain(*13, 15, 30, 35, 36, 57, 61, 62*) - play leading roles in neural synchrony and in brain state transition(*36, 62*). Particularly, GABAergic hub neurons in hippocampal-entorhinal circuits have been shown to drive network dynamics and spontaneously coordinate neuronal synchronization(*61, 63*). Building on previous findings, we demonstrate that hub neurons in the PPC play a primary role in encoding key task variables that mediate an animal's behavioral performance, as well as guiding the activity dynamics and the evolution of neuronal representations during animal's behavior performance and learning. Together, these results suggest that hubs are crucial network structures that significantly contribute to overall brain activity and animal behavior.

Modular organization - a hallmark of small-world networks - enables parallel, specialized processing in the brain(*1, 8, 10, 56*). This architecture has been observed across scales, from macroscopic networks of functionally related brain regions to mesoscopic neuronal circuits(*15, 16, 29, 36, 55-57, 64*). At the macroscopic scale, network modules typically comprise anatomically and/or functionally related brain areas that may support specific behavioral functions, allowing for rapid and efficient information sharing among regions involved in a common set of tasks or responses(*1, 5, 8, 10, 56, 65*). Consistently, we demonstrate that microscale modules in the PPC exhibit similar principles: neurons within the same module showed greater functional similarity (evidenced by shared encoding patterns) and stronger mutual influence on both activity dynamics and neuronal encoding during the monkeys' task performance and learning than those across modules. These results collectively establish modularity as a conserved organizational principle that facilitates functional segregation across different levels of neural computation.

The functional brain network is dynamic, evolving over time(*2, 8, 9, 17, 66*). It has been shown to gradually develop during brain maturation and undergo significant changes across different

behavioral and brain states(*8, 29, 67-69*). Previous study has demonstrated that computing neuron hubs are dynamic, with a neuron's hub status potentially changing across different brain substates or even swapping roles(*62*). Consistent with, and extending previous research, we observed changes in the hub/non-hub status of PPC neurons across days, which was closely correlated with the evolution of neuronal encoding and information flow during long-term learning. Specifically, changes in neurons' hub or non-hub status were associated with shifts in their functional roles during task performance, as the strength of their encoding of key task variables increased after gaining hub status or decreased after losing it. Furthermore, hub-losing neurons exerted a greater influence on the evolution of neuronal encoding of other neurons within the local network, while hub-gaining neurons received stronger influences from other neurons in shaping their neuronal encoding. Notably, these dynamic neurons exhibited a higher proportion of positive (over negative) inter-module connections than neurons with stable hub/non-hub status. This suggests that a neuron's topological transitions—and corresponding changes in information encoding during learning—may be constrained by its involvement in inter-module communication.

Importantly, we found that the small-world topology of PPC neuron networks predicted the monkeys' daily behavioral performance during sensorimotor associative learning. Global neural computation within these networks became increasingly efficient over time, potentially supporting more effective information processing and the emergence of proficient, task-adapted behaviors. Our results indicate a potential principle whereby topological evolution of local circuits drives the refinement of neuronal representations during long-term learning. Supporting this idea, previous fMRI studies have reported increased local efficiency—closely related to local clustering—in the frontal cortex following motor learning(*70*) and in the superior temporal cortex after spoken language learning(*71*). While our findings appear to contrast these results, the discrepancy may be due to differences in spatial scale: our micro-scale measurements versus macroscopic network observations. Differences in brain regions and types of learning may also contribute. Additionally, studies of motor learning have observed diverse topological changes, including increased clustering coefficients, greater connection density and strength, shorter communication paths, and altered centrality(*72, 73*). Future research should investigate whether different types of learning induce distinct network dynamics across spatial scales and brain regions.

Finally, future studies should investigate how network organization differs across neuron types (e.g., excitatory vs. inhibitory), cortical layers, and brain regions. Causal manipulations through targeted single-neuron interventions, combined with structural network mapping, are also essential to uncover how network topology enables interactions among neural elements, providing mechanistic insights into the emergence of diverse forms of neural computation.

Materials and Methods：

Animal preparation and Behavioral Training

The procedures are described in detail in our previous study(*1*), but here we will only provide a brief summary. Two male macaque monkeys, aged 4-5 years and weighing 5-6 kg, were trained on the behavioral task. Prior to the training, three head-posts were implanted on the monkeys'

skulls in an inverted Y-shape configuration. A T-shaped steel frame was then attached to these head-posts to enhance head fixation stability. Our surgical and behavioral methods have been described in detail previously. The monkeys were individually housed in cages and kept under a 12-hour light/dark cycle. Behavioral training and experimental recordings were conducted exclusively during the light phase. The monkeys were seated comfortably and head-fixed in a custom-made primate chair inside a dark experimental rig. Task stimuli were displayed on a 27-inch color LCD monitor (1920x1080 resolution, 75 Hz refresh rate, 45 cm viewing distance). A solenoid-operated reward system was used to deliver juice rewards to the monkeys. Eye positions were monitored using an optical eye tracker (ISCAN ETL-200) at a sampling rate of 240 Hz and stored for offline analysis. Stimulus presentation, task events, rewards, and behavioral data acquisition were controlled by an Intel-based PC running MonkeyLogic software in MATLAB (http://www.monkeylogic.net). All experimental and surgical procedures were approved by the Peking University Animal Care and Use Committee.

Behavioral tasks

Image saccade association learning task (ISAL)

The task sequence and stimuli are described in detail in our previous study(*1*). Briefly, monkeys were trained to associate visual images with two saccade directions in each learning phase. On each trial, they made a saccade to one of two targets based on the presented image (**fig. S1**). Each trial began with a central fixation point, which the monkeys had to maintain until making their saccadic choice. After 1500 ms of fixation, a visual image appeared on the screen's contralateral side (relative to the recorded hemisphere) for 500 ms. Following a 1-second delay, the fixation point disappeared, and two saccade targets appeared simultaneously on the left and right sides of the screen, positioned orthogonally to the image's orientation. Monkeys had to saccade to the target associated with the image within 400 ms and maintain fixation for 1 second to receive a juice reward, delivered immediately after target disappearance. Although no explicit feedback was provided, the monkeys quickly learned trial outcomes (correct or erroneous). Once they mastered one pair of image-saccade associations, they proceeded to learn two novel associations in subsequent sessions.

Task training

The task training sequence is described in detail in our previous study(*1*). During the course of neural recordings, two monkeys learned a total of 12 pairs of novel image-saccade associations (Monkey H: 3 pairs, Monkey X: 11 pairs). This allowed us to consistently track the same neurons across all 12 subregions of area 7a throughout the entire learning process. During each learning phase, the monkeys were initially tested with the ISAL task using previously learned (familiar) associations on the first day. On subsequent days, they were introduced to a new pair of associations until they achieved full proficiency. Importantly, within each recording session, the image-saccade associations remained constant.

Neural recording

Virus injection and chamber implanting

We implemented two-photon calcium imaging recording during monkeys performing the ISAL task, in order to track the neuronal activity across different days. Detailed procedures for the surgical and recording processes are elaborated upon in the previous studies(*1, 2*). In brief, we conducted two surgeries on each animal to inject the virus for transferring the calcium indicator into cortex and to implant the optical recording chamber respectively. During the first surgery, a craniotomy was executed on the skull over area 7a in the right hemisphere of each monkey. We located area 7a according to the monkey brain atlas, specifically situated as the posterior part of the inferior parietal gyrus, located beneath the intraparietal sulcus and above the superior temporal sulcus. Following the dura mater's exposure, we injected 50-100 nL AAV9-Syn-GCaMP6f-WPRE-SV40 into cortex at a depth of approximately 400μm. Approximately 45 days after virus injection, we performed the second surgery to implant the recording chamber. A glass coverslip glued in a titanium ring with silicone adhesive was used to gently cover the cortex.

Two photon calcium imaging recording

The procedures for neural imaging were described in detailed in our previous study(*1*). In brief, we conducted the two-photon calcium imaging recording experiment using a Thorlabs two-photon microscope and a Ti:Sapphire laser (Mai Tai eHP, Spectra Physics) approximately one week after the implantation of the recording chamber. In each recording session, a cortical area of 800 μm × 800 μm was imaged at 30Hz using a 16× objective lens (0.8 N.A., Nikon), and then averaged each 4 frames resulted in 7.5 frames/s. The recording depth ranged from 200 μm to 300 μm beneath the arachnoid membrane. A standard slow galvo scan was used to obtain static images of neurons with high resolution (1024* 1024). Approximately every 5-10 minutes, we manually corrected slow drifts in the field of view (FOV) by comparing them to a reference image. In total, we consistently monitored the activities of the same neurons throughout a full learning course spanning a period of 3 to 7 days within 12 FOVs. This resulted in 59 recording sessions from two monkeys (2 FOVs and 7 recording sessions for Monkey H and 10 FOVs and 52 recording sessions for Monkey X). To ensure alignment with the same imaging plane on consecutive days, we initially performed coarse alignment based on the recording coordinates, blood vessels, pia mater, and arachnoid, followed by precise alignment to reference images.

Data analysis

Behavioral performance

We included only those recording sessions in which the monkeys completed a sufficient number of trials ($n \geq 800$ for Monkey H and $n \geq 700$ for Monkey X) in our subsequent analyses. The monkeys' performance accuracy was calculated as the ratio of correct trials to the total number of completed trials, including both correct and erroneous trials. To determine whether the monkeys had fully acquired a pair of image-saccade associations, we applied two criteria: 1) the monkey's average accuracy throughout the session exceeded 0.8, and 2) the monkey's average accuracy reached 0.9 over a continuous period of at least 200 trials.

Dynamic model fitting

As described in our previous study, we fitted monkeys' performance accuracy with a dynamic Bernoulli generalized linear model, characterized by a set of smoothly evolving psychophysical

weights, in order to capture the dynamics of monkeys' behavior strategies during learning. We used 'PsyTrack' package, which was proven suitable for parametrizing the time-varying behavior in learning task (https:// github.com/nicholas-roy/PsyTrack). This model describes choice behavior at the resolution of single trials, allowing us to quantify the evolution of animal's decision strategies (represented by different weights) across the learning course. Specifically, we utilized the task condition (Cue identity) as input for the model, denoting each single trial as either -1 or 1, while the monkeys' choice (Saccade direction) served as the model's output, labeled as 0 or 1 for each single trial. We determined two behavioral weights, namely the bias weight and stimulus weight, through model fitting.

Neuronal data analysis

Identify single neurons within each session and across sessions during learning

The procedures for identifying single neurons were described in detail in our previous study(*1*). We used an image processing software (suite2p,), for motion correction, definition of putative cell bodies, and extraction of fluorescence traces. We extracted the single neuron activity within each FOV based on three primary steps. First, the raw data streaming from the microscope system was converted into ome.tif format using Fiji software, and then transferred to 'suite2p' for offline processing, which included motion correction, extraction of neuronal signals, and denoising. Second, we manually validated the cell bodies (ROIs) candidates generated from suite2p, and then employed a machine learning approach to optimize parameters tailored to the data recorded from different subregions of area 7a in each monkey. These refined parameters were subsequently applied to 'suite2p' to reprocess the data again, generating new ROIs for each data session. Lastly, we manually inspected and selected ROIs once more to ensure that all identified ROIs exhibited satisfactory neuron morphology and met the quality criteria.

Following the selection of ROIs for each recording session, we proceeded to align the neurons across all the recording sessions\days throughout the learning course for each tested 7a FOVs. This involved the following steps. 1) We utilized 'suite2p' to generate a cross-day classifier by leveraging data from all sessions/days within each learning course for each 7a subregion. 2) Subsequently, we imported the cross-day classifier into 'suite2p' to generate ROIs for each individual day within the learning course. 3) We manually cross-referenced and matched the neurons (ROIs) among different recording sessions within each learning course, based on their spatial location in the reference plane and their morphology. If a neuron could not be confidently identified in one of the sessions within the learning course, it was excluded from consideration for all recording sessions within that learning course. As discussed in detail in our previous study, we have confidence that the observed changes in functional neuron network for each FOV during the learning course are unlikely to be primarily attributable to fluctuations in the recording quality across different recording sessions(*1*).

As described in our previous study(*1*), we implemented a high-pass filter on the fluorescence trace of each neuron, effectively eliminating very slow dynamics within each recording session (High pass filter, 0.005 Hz), in order to mitigate the potential noise resulted from factors such as slow drifts in the imaging plane's focus and light bleaching.

Quantify the encodings of key task variables

Identify outcome selectivity

To identify neurons with significant encoding of trial outcome, we applied a *Wilcoxon Ranksum* test to assess activity between the correct and error trials in the task period following target offset (1-16 frames (0-2.2s) after target offset). We further divided this period into four smaller windows, each comprising 4 frames. If statistically significant differential activity between correct and error trials was observed within at least one of these windows ($P < 0.01$, Bonferroni corrected), we classified the neuron as outcome-selective.

Identify saccade direction selectivity

To identify neurons exhibiting significant saccade direction encoding, we employed a *Wilcoxon Ranksum* test to compare neural activities around saccade onset between trials featuring different saccade directions. Specifically, we assessed saccade direction selectivity during both the pre-saccadic period (1-4 frames before saccade onset) and the post-saccadic phase (1-8 frames after saccade onset). While the pre-saccadic epoch was analyzed as a single time window, we divided the post-saccadic epoch into two smaller time windows (4 frames each). Neurons were classified as saccade selective if there was statistically significant differential activity observed between trials with distinct saccade directions in at least one time window ($P < 0.01$, Bonferroni corrected).

Unbiased fraction of explained variance (FEV)

Similar as in previous studies, we performed one-way ANOVA on the neuron's activity within each time frame to quantify the amount of information that each neuron encoded about trial outcome and saccade direction. We calculated the unbiased fraction of explained variance (FEV) in the neuron's activity that could be attributed to the trial outcome or saccade direction with the following:

$$FEV_{(factor)} = (SS_{(factor)}-(k-1)MSE)/(SS_{(total)} +MSE),$$

where SS indicates the sum of squares, MSE indicates mean square error, and k indicates number of conditions.

Separation Index

To test whether there were differences in encoding different task variables (e.g., saccade and outcome) between different modules within each network, we calculated a separation index (SI), formulated as follows:

$$SI(i,j) = \frac{|V_2(i) - V_1(j)| + |V_1(i) - V_2(j)|}{|V_1(i) - V_1(j)| + |V_2(i) - V_2(j)|}$$

where i and j represent two different neurons, $V_1(i)$ is the encoding strength of variable 1 for neuron i, and $V_2(i)$ represents the encoding strength of the second task variable for neuron i. The SI quantifies the degree to which two task variables are separately encoded across different modules within the network. Specifically, we used the highest FEV value from all time windows to measure the strength of neuronal encoding for each task variable ($V_1(i)$) for a given neuron.

Construct the functional neuron network

Generating the connection matrix

We quantified the connectivity between simultaneously recorded neurons using partial noise correlation, following these steps: 1) Single-trial responses were estimated by averaging the activity within three time windows (1-4 frames, 5-8 frames, and 9-12 frames before cue onset) during the fixation periods of the ISAL task. 2) A partial correlation algorithm was then applied to the neuron-by-trial matrix to compute correlations for each neuron pair, excluding the influence of all other neurons. 3) The resulting correlation matrix was thresholded based on the p-value of the partial correlations, retaining pairs with $p < 0.001$ and setting the rest to zero. 4) The diagonals of the matrix were set to zero to prevent self-connections. This undirected matrix was then used as the weighted adjacency matrix in the subsequent graph-based analysis.

We used the Brain Connectivity Toolbox (*3*) to analyze the resulting functional neuron network and calculate different network properties, with specific details outlined below: The length matrix was constructed using the inverse of the absolute value of the connection weights. The positive connection weights were used to calculate the strength of the nodes and to perform the core-periphery analysis. For community detection, the original weight values (including negative connections) were considered.

Examine Factors on connection weights

We used linear regression to examine if the connection weights in the PPC neuron networks could be predicted using functional similarity or spatial proximity:

$$E_{ij} = b_0 + b_1 S_{ij} + b_2 D_{ij}$$

Where E_{ij} is the connection weight between node I and node j, S_{ij} is the signal correlation between neuron i and j, D_{ij} is the distance between neuron i and j. The coefficients $\{b_0, b_1, b_2\}$ are regression coefficients. This linear regression is done based on each session's data.

Small-world topology

Quantify small-worldness

To quantify the extent to which the 7a neuron network exhibited small-world topology, we calculated the small-world coefficient σ as follows:

$$\sigma = CC_{norm}/\lambda_{norm},$$

$$CC_{norm} = CC/CC_{random},$$

$$\lambda_{norm} = \lambda/\lambda_{random}$$

Where CC_{norm} is the normalized clustering coefficient, defined as the ratio of the actual clustering coefficient to that of a strength-preserving random network. The clustering coefficient is defined as the number of closed triplets over the total number of triplets. In a network with signed and weighted connections, CC is calculated as:

$$CC = \frac{\sum_i \sum_{j,q} w_{ij} w_{iq} w_{jq}}{\sum_i \sum_{j \neq q} |w_{ij} w_{iq}| + \sum_{ij} {w_{ij}}^2}$$

Where w_{ij} represents the connection weight between node i and node j. This means that balanced triads (with an even number of negative edges) increase the clustering coefficient, while unbalanced triads (with an odd number of negative edges) decrease it. A. $CC_{norm} > 1$ indicates high local connectivity in the network.λ_{norm} denotes the normalized characteristic path length, defined as the ratio of the actual characteristic path length of the network to the characteristic path length of a strength-preserving random network. The characteristic path length is defined as the average shortest path length for all possible pairs of nodes in a network. The λ is computed using the length matrix as follows:

$$\lambda = \frac{\sum_i \sum_{j \neq i} d_{ij}}{n(n-1)}$$

Where n is the number of all connected nodes, and d_{ij} is the distance between node I and j. $\lambda_{norm} \approx 1$ means decent global reachability for the network. If $\sigma > 1$, the neuron network is considered to exhibit small-world topology.

All the random networks were constructed to match the strength distribution of the original network. To achieve this, we used the connection-switching method outlined in previous research(*4*). We performed 1000 randomization iterations and calculated the average coefficient across these networks, which was then used as the coefficient value for the null model.

Identify hub and non-hubs within network

As mentioned before, we used the Kernighan-Lin algorithm of core-periphery partitioning in the Brain Connectivity toolbox to detect hub\non-hub organization of the neuron network. The hubs(core) and non-hubs(periphery) partition is based on coreness statistic, which measures the connection density within two groups at the same time. By maximizing the coreness statistic, we get a partition that has within-hub connection as many as possible while making within-non-hub connection as less as possible. The coreness statistic can be formulated as follows:

$$Q_{core} = \frac{\sum_{ij} \delta_{ij} (w_c - \gamma p)}{N_e},$$

$$\delta_{ij} = \begin{cases} +1, & node\ i\ and\ j\ are\ both\ hubs \\ -1, & node\ i\ and\ j\ are\ neither\ hubs, \\ 0 & otherwise \end{cases}$$

$$p = \frac{2N_e}{n^2}$$

Where w_{ij} is the connection weight between node (neuron) i and node j. N_e is the total number of edges in the network, and n is the total number of nodes. γ is the resolution parameter for core/periphery ratio, which we use the conventional value $\gamma = 1$ (similar group size for hub and non-hub nodes).

We constructed the neuron network and calculated the core-periphery partitioning independently for each recording session. As a result, some neurons within each FOV may change their hub/non-hub status across sessions. Neurons that were identified as hubs in one session but transitioned to non-hubs in the subsequent session are referred to as hub-losing neurons, while neurons that gained hub status in the following session are termed hub-gaining neurons.

Identify modular architecture within network

Similarly, we applied the Louvain algorithm from the Brain Connectivity Toolbox to detect the modular (community) organization of each network. The modular (community) partition is based on the modularity statistic, which compares the number of inter-module connections to intra-module connections for any given partition. Maximizing the modularity statistic leads to a higher number of intra-module connections and fewer inter-module connections. For signed networks, we employed the generalized modularity statistic, which is formulated as follows:

$$Q_{mod} = \frac{1}{v^+}\sum_{ij}(w_{ij}^+ - \gamma e_{ij}^+)\delta(M_i, M_j) - \frac{1}{v^+ + v^-}\sum_{ij}(w_{ij}^+ - \gamma e_{ij}^+)\delta(M_i, M_j)$$

Where $w_{ij}^{\pm}$ is the positive/negative connection weight between node i and node j, and $v^{\pm}$ is the sum of all positive/negative weights, which is formulated as follows:

$$v^{\pm} = \sum_{ij} w_{ij}^{\pm}$$

The $e_{ij}^{\pm}$ is the expected value of connection weight by chance, which is formulated as follows:

$$e_{ij}^{\pm} = \frac{\sum_{ik} w_{ik}^{\pm} \sum_{jk} w_{jk}^{\pm}}{v^{\pm}}$$

$\delta(M_i, M_j)$ denotes whether these neurons belongs to the same modular, which is formulated as follows：

$$\delta(M_i, M_j) = \begin{cases} 1, & M_i = M_j \\ 0, & M_i \neq M_j \end{cases}$$

where M_i is the modular index of node i. The γ is resolution parameter for module (community) size. We used the conventional value $\gamma = 1$.

Due to modular degeneracy (a network can have multiple partitions that have comparable high modularity), we run Louvain algorithm for 1000 times to get an estimate of modularity value Q_{mod} and the probability that two node i,j are in the same module $P(M_i = M_j)$. Analysis based on module partition were done with each partition and then averaged (**Fig. 4**) or based on the probability.

To further examine topological positions of different neuron subsets, we calculated the diversity coefficient, measuring a node's connections to communities outside of its own community normalized by its within-community (inter-module connections relative to its within-module

connections). The normalized connection diversity in a given modular partition M, based on Shannon entropy, is formulated as:

$$h_i^{\pm} = -\frac{1}{\log(m)} \sum_{u \in M} \frac{s_i^{\pm}(u)}{s_i^{\pm}} \log\left(\frac{s_i^{\pm}(u)}{s_i^{\pm}}\right)$$

Where $s_i^{\pm}$ is the positive/negative connection strength of node i, and $s_i^{\pm}(u)$ is the positive/negative connection strength of node i within module u.

Comparison with random network

We compare the 7a neuron networks with several types of random networks (null models) to evaluate their properties. First, we compare the degree distribution of our network with that of an a Erdős–Rényi network which is a random network having the same number of nodes and equal connection probability for each pair of nodes. The degree distribution of such random networks is known to follow a binomial distribution (or Poisson distribution for sufficiently large node numbers).

To assess the statistical significance of the modular structure in our network, we compare it with a random network that matches the degree distribution, connection weight, and strength distribution of the original network. We generate these random networks using the connection-switching method in the Brain Connectivity Toolbox. We construct 1000 random networks in this manner and calculate their modularity value, Q_{modr}. If the normalized modularity $\frac{Q_{mod}}{Q_{modr}}$, was greater than 1 for the 95% random networks, the network is considered to exhibit a significant modular structure.

Similarly, we define the statistical significance of the core/periphery partition by comparing it with an Erdős–Rényi network. Since we use a weighted version of the coreness statistic, we also generate the null distribution of connection weights as follows:

We compute the partial noise correlation of the neuron-by-trial matrix, with the trial indices shuffled for each neuron. We then apply the same threshold ($p < 1/1000$) to the correlation matrix to obtain the adjacency matrix. These random matrices are much sparser than the real data, so we bootstrap with 100 matrices and use all existing edges to create a new matrix that has a similar edge count to the real data. We repeat this process 1000 times to estimate the coreness value Q_{core_r}. If the normalized coreness $\frac{Q_{core}}{Q_{core_r}}$ was greater than 1 for the 95% random networks, the network is considered to have a significant core/periphery structure (hub/non-hub topology).

We used generalized linear regression to test whether physiological features of any given neuron (luminance & size) could determine the hub status of the corresponding node in certain networks as following:

$$\log(P(H_i)/(1 - P(H_i))) = b_0 + b_1 L_i + b_2 S_i + b_3 C_i$$

Here the $P(H_i)$ is the probability of node i being hub, L_i is the luminance of cell i, S_i is the size (in pixel^2) of cell i and C_i is the connection strength of node i in that particular network. The coefficients $b_0 \sim b_3$ are regression coefficients. This regression is applied individually for each recording session.

Spatial layout of Hub/non-hub

We applied two different analyses to test whether or not the hub/non-hub groups are spatially overlapped. These analyses are all done separately on the network from each recording session.

First, we calculated the receiver operating characteristic curve (ROC) with distance between neuron pairs as predictor and within/across group (hub\non-hub) as conditions. Ideally, if the hub/non-hub groups were spatially separated, then the neuron pairs would drastically shift from within group to across group as the distance increase. We use the area under curve (AUC) value as the measurement of spatial separation.

We also used the Dunn Index (DI) to examine if the hub/non-hub neurons were forming spatial clusters. Dunn Index is formulated as follows:

$$DI = \min_{1\le i\le c}\left\{\min_{1\le j\le c, j\neq i}\left\{\frac{\delta(X_i, X_j)}{\max_{1\le k\le c}\Delta(X_k)}\right\}\right\}$$

Where c is the total number of clusters (c=2), $\delta(X_i, X_j)$ is the inter-cluster distance of cluster X_i and X_j ,$\Delta(X_k)$ is the intra-cluster distance of cluster X_k. High DI indicates better distinction, low DI indicates no distinction.

Spatial layout of modules

We calculated a spatial clustering index based on both the modular partition and spatial position of each neuron. The spatial clustering index is defined as:

$$CI(d) = \frac{E(1-\rho_{resampled})}{E(1-\rho_{actual}|d)}$$

Where ρ is the probability of certain neuron pairs being in the same module, and d is the spatial distance between those neuron pairs. The distance d was discretized into 50 μm bins from 0 to 800 μm. The spatial clustering index was computed for pairs of neurons whose distances fell within each distance bin. The $\rho_{resampled}$ was calculated using bootstrap (1000 times).

Spatial clustering index values greater than 1 indicate that those neurons are more likely to be in the same module than chance, whereas values smaller than 1 indicate that those neurons are more likely to be in the same module than chance. The significance of spatial clustering index is determined by comparing the observed result to a shuffled distribution (bootstrap size = 1000). A result is deemed statistically significant when the CI exceeds the values found in 99.9% of the

shuffled results, indicating that it is significantly different from chance. The spatial clustering index is also calculated based on each single session's data.

Quantify the influence of single neuron on the activity dynamics within network

Signal correlation

To quantify the similarity in neuronal encodings of task variables between neurons identified within the same session or across different sessions, we calculated the signal correlation for each pair of neurons. Unlike classical methods, we incorporated both time and trial conditions into the calculation of signal correlation. Specifically, we first constructed the condition-averaged activity vector $A \in v^{c_1 c_2 t}$, where c_1 denotes two saccadic conditions (left and right), c_2 denotes two outcome conditions (correct and error), and t denotes time (1-12 imaging frame before cue onset, 12 imaging frame between cue onset and saccade onset, 8 imaging frame between saccade and target offset, and 1-16 imaging frame after the target offset). The signal correlation between each pair of neurons was defined as the Pearson correlation between their respective activity vectors. We computed signal correlations for outcome encoding and saccade encoding separately, using different time periods: for outcome encoding, we used the 1-16 imaging frames after target offset; for saccade encoding, we used the 1-8 imaging frames before saccade onset and the 1-8 imaging frames after saccade onset.

Noise correlation

Noise correlations between different neurons were calculated using the neural activity in fixation time period of the ISAL task as for partial noise correlations. Specifically: 1) Single-trial responses were estimated by averaging the activity within three time windows (1-4 frames, 5-8 frames, and 9-12 frames before cue onset) during the ISAL task. 2) Pearson correlations were computed by calculating the pairwise trial-by-trial activity for each neuron pair.

Correlation of changes in neural selectivity

Selectivity changes are defined as the difference in activity vectors between two successive recording sessions or between the first and second halves of a given session. The correlation of selectivity changes between two neurons was calculated by computing the Pearson correlation between their respective differences in activity vectors.

Principle component (PC) Index

To examine the contribution of each neuron to the populational activity dynamics within each network, we calculated a PC index, which is formulated as follows:

$$PI(k) = \sum_{n=1}^{10} C(n,k)S(n)$$

where, $C(n,k)$ is the absolute loading of neuron k in top component n, and $S(n)$ is the explained variance of top component n. The PC Index for a given group of neurons is the average PC Index of those neurons.

Causality index

To test the effect of different neurons on the activity dynamics within a local neuron network, we quantified the influence of each neuron's activity during a given time period on the activity of other neurons in subsequent time periods within the same trial. We introduced a new metric, called the causality index (CI), which is formulated as follows:

$$CI(i,j;k) = r_t((A(j,t+k), A(i,t))|A(j,t))$$

where i and j denote different neurons, k is the time lag, $A(i,t)$ represents the activity of neuron i at time point t during a trial, and $r_t(x_t, y_t|z_t)$ is the partial correlation between x and y while controlling for z, where x, y, and z are time-dependent variables, and t spans all relevant time points within a trial. Thus, $CI(i,j;k)$ quantifies the partial correlation between the activity of neuron i and the activity of neuron j after k frames, given the activity of neuron j at the current time. This measures the influence of neuron i on neuron j's activity after a time lag of k frames, while excluding the effect of each neuron's own prior activity on its later activity.

Additionally, we used the causality index to quantify the influence of each neuron on changes in neuronal selectivity within the network across different learning periods. Specifically, we represented neuronal selectivity for each neuron using the activity vector $A \in v^{c_1 c_2 t}$. In this context, the causality index measures how strongly one neuron drives another's selectivity toward or away from its own selectivity across different learning periods.

Quantify the evolution of population activity

Alignment index

To quantify the relationship between the population codes for trial outcome across different days, we calculated the alignment index (AI), similar as in the previous study(*1*). We quantified the degree of alignment/overlap between the neural subspaces of the population activity from different days within each learning course, and tested how these neural subspaces, responsible for encoding trial outcomes or saccade direction, evolved throughout the learning course.

To calculate AI, we first constructed the population activity matrix $P_i \in R^{N \times CT}$ for each day, where N is the total number of neurons, C is the numbers of conditions and T is the numbers of time points. Subsequently, to calculate the AI between day i and day j ($A(i,j)$), we conducted principal component analysis (PCA) on activity matrix P_i to obtain the PCs of day i, considering each neuron as a variable. We selected the top 10 PCs to form a 10-dimensonal orthogonal axis in N-dimensional neural space. The degree of overlap between neural subspaces can be estimated by projecting the activity matrix from day j onto the PCs of day i and quantifying the proportion of variance explained relative to the total variance of population activity on day j. Thus, we defined the alignment index $A(i,j)$ as:

$$A(i,j) = \frac{Tr(D_{day\ i}^T C_{day\ j} D_{day\ i})}{\sum_{k=1}^{10} \sigma_{day\ j}(k)}$$

Where $D_{day\ i}$ is the top 10 eigenvectors obtained by PCA. $C_{day\ j}$ is the covariance of matrix P_j. $\sigma_{day\ j}(k)$ is the k-th singular value of $C_{day\ j}$. The $Tr()$ function denotes the matrix trace, which sums along the diagonal entry. The reverse, $A(j,i)$, can be calculated in similar ways. The numerator quantifies the proportion of variance in population activity from day j that is captured by the top ten PCs of day i. The denominator normalizes the alignment index with respect to the maximum amount of variance in population activity from day j that can be explained by a ten-dimensional subspace (i.e., the variance captured by the top ten PCs of day j). As a result, the AI ranged from 0, indicating perfect orthogonality, to 1, signifying perfect alignment.

Prediction of the similarity of neuronal encoding between neurons

To further investigate how small-world network topology influences the functional roles of PPC neurons and shapes activity evolution during learning, we tested whether the topological position of neurons could predict the similarity of their neural encodings. We quantified this similarity using signal correlation. Specifically, we employed a linear model incorporating four parameters of network topology to predict the signal correlation between each pair of recorded neurons within each PPC network as follows:

$$C_{signal}\ (i,j) = \beta_1\ H(i,j) + \beta_2 P(M(i,j)) + \beta_3 W(i,j) + \beta_4 N(i,j) + b$$

where $H(i,j)$ denotes the hub and non-hub status of the neurons, formulated as:

$$H(i,j) = Hub(i) + Hub(j) - 1,\ \ Hub(k) = \begin{cases} 1, & \text{k is Hub} \\ 0, & \text{k is not Hub} \end{cases}$$

$P(M(i,j))$ denotes the probability that two neurons are in the same module.

$W(i,j)$ represents the relative connection weight between neurons, formulated as:

$$W(i,j) = \frac{w_{ij}}{\sqrt{\sum_k w_{ik} \times \sum_k w_{jk}}}$$

Where w_{ij} is the connection weight between neuron i and j.

$N(i,j)$ denotes the weighted topological overlap between neurons, formulated as:

$$N(i,j) = \frac{w_{ij} + \sum_{k \neq i,j} w_{ik} w_{kj}}{\min\left(\sum_k w_{ik}, \sum_k w_{jk}\right) + 1 - w_{ij}}$$

Where w_{ij} is the connection weight between neuron i and j.

In order to capture detailed connectivity structure within each neuron network, we did not thresholding the connection matrix before computing modular and hub/non-hub status in this analysis. Furthermore, we shuffled the neuron id j for $C_{signal}\ (i,j)$ before doing regression for control analysis.

Quantify the relationship between network topology and the monkeys' daily performance during learning.

To capture the dynamics of the monkeys' choice strategies during learning, we fitted their performance accuracy using a dynamic Bernoulli generalized linear model ("PsyTrack"), characterized by a set of smoothly evolving psychophysical weights. The goal of this model is to estimate weights that reflect the animals' decision-making strategies on a trial-by-trial basis, using a linear combination of relevant task variables. This approach allows us to quantify how the monkeys' decision strategies, represented by these weights, evolve across learning periods. Importantly, the magnitude of each weight indicates how strongly the animal relies on the corresponding task variable in its decision-making process. Consistent with our previous study, we used the cue identity as the input to the model and the monkeys' saccade choice as the output. From this, we derived two behavioral weights: the bias weight and the stimulus weight. These weights represent the extent to which the monkeys' saccade choices were influenced by internal bias (toward the ipsilateral target relative to the recorded hemisphere) and the visual stimulus, respectively. We then averaged the decision weights for each day to represent the monkeys' behavioral performance on that day.

Next, we applied generalized linear regression models to fit the monkeys' daily performance accuracy, as well as the daily averaged stimulus weight and bias weight, using network topology parameters as predictors. Stepwise regression guided by the Bayesian Information Criterion (BIC) was applied to select the most informative variables. Six network topology measures were considered as candidate regressors: rightward skew of the edge weight distribution (modeled by the Generalized Extreme Value distribution), connection density, clustering coefficient, characteristic short-path length, coreness, and modularity. The initial models included an intercept and a linear term for each predictor, and terms were subsequently added or removed one at a time based on their impact on the BIC value. This analysis yielded regression formulas incorporating only the significant predictors, as detailed below:

$$\bar{W}_{accuracy} = \beta_1 Q_{mod} + \beta_2 SPL + \beta_3 Q_{mod} * SPL + b$$

$$\bar{W}_{bias} = \beta_1 Den + \beta_2 Q_{mod} + \beta_3 SPL + b$$

$$\bar{W}_{stimulus} = \beta_1 Q_{mod} + \beta_2 SPL + \beta_3 Q_{mod} * SPL + b$$

Where $\bar{W}_{accuracy}$ denotes the averaged performance accuracy for a given day, $\bar{W}_{bias}$ and $\bar{W}_{stimulus}$ represents the average bias weight and stimulus weight, respectively. Q_{mod} is the modularity of the network, *SPL* refers to the average short-path length; and *Den* denotes the average connection density of the network. For the permutation test, we shuffled the learning-day identities for W_{accuracy}, W_{bias}, and W_{stimulus} before performing the regression, as a control analysis.

References and Notes

1 Bassett, D. S. & Bullmore, E. T. Small-world brain networks. *Neuroscientist* **12**, 512-523, doi:10.1177/1073858406293182 (2006).

2 Bressler, S. L. Large-scale cortical networks and cognition. *Brain Res Brain Res Rev* **20**, 288-304, doi:10.1016/0165-0173(94)00016-i (1995).

3 Bullmore, E. & Sporns, O. Complex brain networks: graph theoretical analysis of structural and functional systems. *Nature reviews. Neuroscience* **10**, 186-198, doi:10.1038/nrn2575 (2009).

4 Bullmore, E. & Sporns, O. The economy of brain network organization. *Nature reviews. Neuroscience* **13**, 336-349, doi:10.1038/nrn3214 (2012).

5 Sporns, O. Structure and function of complex brain networks. *Dialogues Clin Neurosci* **15**, 247-262, doi:10.31887/DCNS.2013.15.3/osporns (2013).

6 Sporns, O. & Betzel, R. F. Modular Brain Networks. *Annu Rev Psychol* **67**, 613-640, doi:10.1146/annurev-psych-122414-033634 (2016).

7 van den Heuvel, M. P. & Sporns, O. Network hubs in the human brain. *Trends Cogn Sci* **17**, 683-696, doi:10.1016/j.tics.2013.09.012 (2013).

8 Yuste, R., Cossart, R. & Yaksi, E. Neuronal ensembles: Building blocks of neural circuits. *Neuron* **112**, 875-892, doi:10.1016/j.neuron.2023.12.008 (2024).

9 McIntosh, A. R. Towards a network theory of cognition. *Neural Netw* **13**, 861-870, doi:10.1016/s0893-6080(00)00059-9 (2000).

10 Bassett, D. S. & Sporns, O. Network neuroscience. *Nat Neurosci* **20**, 353-364, doi:10.1038/nn.4502 (2017).

11 He, Y. & Evans, A. Graph theoretical modeling of brain connectivity. *Curr Opin Neurol* **23**, 341-350, doi:10.1097/WCO.0b013e32833aa567 (2010).

12 Avena-Koenigsberger, A., Misic, B. & Sporns, O. Communication dynamics in complex brain networks. *Nature reviews. Neuroscience* **19**, 17-33, doi:10.1038/nrn.2017.149 (2017).

13 Hadjiabadi, D. & Soltesz, I. From single-neuron dynamics to higher-order circuit motifs in control and pathological brain networks. *J Physiol* **601**, 3011-3024, doi:10.1113/JP282749 (2023).

14 Power, J. D., Schlaggar, B. L., Lessov-Schlaggar, C. N. & Petersen, S. E. Evidence for hubs in human functional brain networks. *Neuron* **79**, 798-813, doi:10.1016/j.neuron.2013.07.035 (2013).

15 Bassettt, D. S., Meyer-Lindenberg, A., Achard, S., Duke, T. & Bullmore, E. T. Adaptive reconfiguration of fractal small-world human brain functional networks. *Proceedings of the National Academy of Sciences of the United States of America* **103**, 19518-19523, doi:10.1073/pnas.0606005103 (2006).

16 Hagmann, P. *et al.* Mapping the structural core of human cerebral cortex. *PLoS Biol* **6**, e159, doi:10.1371/journal.pbio.0060159 (2008).

17 He, Y., Chen, Z. J. & Evans, A. C. Small-world anatomical networks in the human brain revealed by cortical thickness from MRI. *Cereb Cortex* **17**, 2407-2419, doi:10.1093/cercor/bhl149 (2007).

18 Liao, X. H., Vasilakos, A. V. & He, Y. Small-world human brain networks: Perspectives and challenges. *Neurosci Biobehav R* **77**, 286-300, doi:10.1016/j.neubiorev.2017.03.018 (2017).

19 Felleman, D. J. & Van Essen, D. C. Distributed hierarchical processing in the primate cerebral cortex. *Cereb Cortex* **1**, 1-47, doi:10.1093/cercor/1.1.1-a (1991).

20 Lewis, J. W. & Van Essen, D. C. Corticocortical connections of visual, sensorimotor, and multimodal processing areas in the parietal lobe of the macaque monkey. *J Comp Neurol* **428**, 112-137, doi:10.1002/1096-9861(20001204)428:1<112::aid-cne8>3.0.co;2-9 (2000).

21 Achard, S., Salvador, R., Whitcher, B., Suckling, J. & Bullmore, E. A resilient, low-frequency, small-world human brain functional network with highly connected association cortical hubs. *J Neurosci* **26**, 63-72, doi:10.1523/JNEUROSCI.3874-05.2006 (2006).

22 Bassett, D. S. *et al.* Hierarchical organization of human cortical networks in health and schizophrenia. *J Neurosci* **28**, 9239-9248, doi:10.1523/JNEUROSCI.1929-08.2008 (2008).

23 van den Heuvel, M. P., Stam, C. J., Boersma, M. & Hulshoff Pol, H. E. Small-world and scale-free organization of voxel-based resting-state functional connectivity in the human brain. *Neuroimage* **43**, 528-539, doi:10.1016/j.neuroimage.2008.08.010 (2008).

24 Stam, C. J. & Reijneveld, J. C. Graph theoretical analysis of complex networks in the brain. *Nonlinear Biomed Phys* **1**, 3, doi:10.1186/1753-4631-1-3 (2007).

25 Carrillo-Reid, L. *et al.* Identification of Pattern Completion Neurons in Neuronal Ensembles Using Probabilistic Graphical Models. *J Neurosci* **41**, 8577-8588, doi:10.1523/JNEUROSCI.0051-21.2021 (2021).

26 Albert, R. & Barabási, A. L. Statistical mechanics of complex networks. *Rev Mod Phys* **74**, 47-97, doi:DOI 10.1103/RevModPhys.74.47 (2002).

27 Borgatti, S. P. Centrality and network flow. *Soc Networks* **27**, 55-71, doi:10.1016/j.socnet.2004.11.008 (2005).

28 Jeong, H., Mason, S. P., Barabasi, A. L. & Oltvai, Z. N. Lethality and centrality in protein networks. *Nature* **411**, 41-42, doi:10.1038/35075138 (2001).

29 Scholz, J., Klein, M. C., Behrens, T. E. & Johansen-Berg, H. Training induces changes in white-matter architecture. *Nat Neurosci* **12**, 1370-1371, doi:10.1038/nn.2412 (2009).

30 30 Bassett, D. S. *et al.* Dynamic reconfiguration of human brain networks during learning. *Proceedings of the National Academy of Sciences of the United States of America* **108**, 7641-7646, doi:10.1073/pnas.1018985108 (2011).

31 Agetsuma, M. *et al.* Activity-dependent organization of prefrontal hub-networks for associative learning and signal transformation. *Nat Commun* **14**, 5996, doi:10.1038/s41467-023-41547-5 (2023).

32 Caroni, P., Donato, F. & Muller, D. Structural plasticity upon learning: regulation and functions. *Nature Reviews Neuroscience* **13**, 478-490, doi:10.1038/nrn3258 (2012).

33 Draganski, B. & May, A. Training-induced structural changes in the adult human brain. *Behav Brain Res* **192**, 137-142, doi:10.1016/j.bbr.2008.02.015 (2008).

40 34 Bassett, D. S., Yang, M., Wymbs, N. F. & Grafton, S. T. Learning-induced autonomy of sensorimotor systems. *Nat Neurosci* **18**, 744-751, doi:10.1038/nn.3993 (2015).

35 Rioult-Pedotti, M. S., Friedman, D. & Donoghue, J. P. Learning-induced LTP in neocortex. *Science* **290**, 533-536, doi:10.1126/science.290.5491.533 (2000).

36 Yu, S., Huang, D., Singer, W. & Nikolic, D. A small world of neuronal synchrony. *Cereb Cortex* **18**, 2891-2901, doi:10.1093/cercor/bhn047 (2008).

37 Dann, B., Michaels, J. A., Schaffelhofer, S. & Scherberger, H. Uniting functional network topology and oscillations in the fronto-parietal single unit network of behaving primates. *Elife* **5**, doi:10.7554/eLife.15719 (2016).

38 Sporns, O. & Zwi, J. D. The small world of the cerebral cortex. *Neuroinformatics* **2**, 145-162, doi:10.1385/NI:2:2:145 (2004).

39 Latora, V. & Marchiori, M. Efficient behavior of small-world networks. *Phys Rev Lett* **87**, 198701, doi:10.1103/PhysRevLett.87.198701 (2001).

40 Watts, D. J. & Strogatz, S. H. Collective dynamics of 'small-world' networks. *Nature* **393**, 440-442, doi:Doi 10.1038/30918 (1998).

41 Zhou, Y. & Freedman, D. J. Posterior parietal cortex plays a causal role in perceptual and categorical decisions. *Science* **365**, 180-185, doi:10.1126/science.aaw8347 (2019).

42 Zhou, Y., Liu, Y., Lu, H., Wu, S. & Zhang, M. Neuronal representation of saccadic error in macaque posterior parietal cortex (PPC). *Elife* **5**, doi:10.7554/eLife.10912 (2016).

43 Zhou, Y., Liu, Y., Wu, S. & Zhang, M. Neuronal Representation of the Saccadic Timing Signals in Macaque Lateral Intraparietal Area. *Cereb Cortex* **28**, 2887-2900, doi:10.1093/cercor/bhx166 (2018).

44 Zhou, Y., Liu, Y. & Zhang, M. Neuronal Correlates of Many-To-One Sensorimotor Mapping in Lateral Intraparietal Cortex. *Cereb Cortex*, doi:10.1093/cercor/bhaa145 (2020).

45 Zhou, Y., Mohan, K. & Freedman, D. J. Abstract Encoding of Categorical Decisions in Medial Superior Temporal and Lateral Intraparietal Cortices. *J Neurosci* **42**, 9069-9081, doi:10.1523/JNEUROSCI.0017-22.2022 (2022).

46 Zhou, Y., Zhu, O. & Freedman, D. J. Posterior Parietal Cortex Plays a Causal Role in Abstract Memory-Based Visual Categorical Decisions. *J Neurosci* **43**, 4315-4328, doi:10.1523/JNEUROSCI.2241-22.2023 (2023).

47 Andersen, R. A., Essick, G. K. & Siegel, R. M. Encoding of spatial location by posterior parietal neurons. *Science* **230**, 456-458, doi:10.1126/science.4048942 (1985).

48 Andersen, R. A. & Buneo, C. A. Intentional maps in posterior parietal cortex. *Annu Rev Neurosci* **25**, 189-220, doi:10.1146/annurev.neuro.25.112701.142922 (2002).

49 Freedman, D. J. & Assad, J. A. Neuronal Mechanisms of Visual Categorization: An Abstract View on Decision Making. *Annu Rev Neurosci* **39**, 129-147, doi:10.1146/annurev-neuro-071714-033919 (2016).

50 Gold, J. I. & Shadlen, M. N. The neural basis of decision making. *Annu Rev Neurosci* **30**, 535-574, doi:10.1146/annurev.neuro.29.051605.113038 (2007).

51 Huk, A. C., Katz, L. N. & Yates, J. L. The Role of the Lateral Intraparietal Area in (the Study of) Decision Making. *Annu Rev Neurosci* **40**, 349-372, doi:10.1146/annurev-neuro-072116-031508 (2017).

52 Liu, Z., Jiang, Z., Shi, L., Fang F., Tang S., & Zhou, Y. . Neural Correlates of Trial Outcome Monitoring during Long-term Learning in Primate Posterior Parietal Cortex. *BioRxiv* (2025).

53 Poli, D., Pastore, V. P., Martinoia, S. & Massobrio, P. From functional to structural connectivity using partial correlation in neuronal assemblies. *J Neural Eng* **13**, 026023, doi:10.1088/1741-2560/13/2/026023 (2016).

54 Roy, N. A. *et al.* Extracting the dynamics of behavior in sensory decision-making experiments. *Neuron* **109**, 597-610 e596, doi:10.1016/j.neuron.2020.12.004 (2021).

55 Chen, Z. J., He, Y., Rosa-Neto, P., Germann, J. & Evans, A. C. Revealing modular architecture of human brain structural networks by using cortical thickness from MRI. *Cereb Cortex* **18**, 2374-2381, doi:10.1093/cercor/bhn003 (2008).

56 Meunier, D., Lambiotte, R. & Bullmore, E. T. Modular and hierarchically modular organization of brain networks. *Front Neurosci* **4**, 200, doi:10.3389/fnins.2010.00200 (2010).

57 Shimono, M. & Beggs, J. M. Functional Clusters, Hubs, and Communities in the Cortical Microconnectome. *Cereb Cortex* **25**, 3743-3757, doi:10.1093/cercor/bhu252 (2015).

58 van den Heuvel, M. P. & Sporns, O. Rich-Club Organization of the Human Connectome. *Journal of Neuroscience* **31**, 15775-15786, doi:10.1523/Jneurosci.3539-11.2011 (2011).

59 van den Heuvel, M. P. & Sporns, O. An Anatomical Substrate for Integration among Functional Networks in Human Cortex. *Journal of Neuroscience* **33**, 14489-+, doi:10.1523/Jneurosci.2128-13.2013 (2013).

60 Song, S., Sjöstrom, P. J., Reigl, M., Nelson, S. & Chklovskii, D. B. Highly nonrandom features of synaptic connectivity in local cortical circuits. *Plos Biology* **3**, 507-519, doi:ARTN e6810.1371/journal.pbio.0030068 (2005).

61 Modol, L. *et al.* Spatial Embryonic Origin Delineates GABAergic Hub Neurons Driving Network Dynamics in the Developing Entorhinal Cortex. *Cereb Cortex* **27**, 4649-4661, doi:10.1093/cercor/bhx198 (2017).

62 Clawson, W. *et al.* Computing hubs in the hippocampus and cortex. *Sci Adv* **5**, eaax4843, doi:10.1126/sciadv.aax4843 (2019).

63 Schroeter, M. S., Charlesworth, P., Kitzbichler, M. G., Paulsen, O. & Bullmore, E. T. Emergence of rich-club topology and coordinated dynamics in development of hippocampal functional networks in vitro. *J Neurosci* **35**, 5459-5470, doi:10.1523/JNEUROSCI.4259-14.2015 (2015).

64 Kashtan, N. & Alon, U. Spontaneous evolution of modularity and network motifs. *Proceedings of the National Academy of Sciences of the United States of America* **102**, 13773-13778, doi:10.1073/pnas.0503610102 (2005).

65 Valencia, M. *et al.* Complex modular structure of large-scale brain networks. *Chaos* **19**, 023119, doi:10.1063/1.3129783 (2009).

66 Tang, D., Zylberberg, J., Jia, X. & Choi, H. Stimulus-dependent functional network topology in mouse visual cortex. *bioRxiv*, doi:10.1101/2023.07.03.547364 (2023).

67 Meunier, D., Achard, S., Morcom, A. & Bullmore, E. Age-related changes in modular organization of human brain functional networks. *Neuroimage* **44**, 715-723, doi:10.1016/j.neuroimage.2008.09.062 (2009).

68 Liu, X. & Duyn, J. H. Time-varying functional network information extracted from brief instances of spontaneous brain activity. *Proceedings of the National Academy of Sciences of the United States of America* **110**, 4392-4397, doi:10.1073/pnas.1216856110 (2013).

69 Calhoun, V. D., Miller, R., Pearlson, G. & Adali, T. The chronnectome: time-varying connectivity networks as the next frontier in fMRI data discovery. *Neuron* **84**, 262-274, doi:10.1016/j.neuron.2014.10.015 (2014).

70 Ma, L., Narayana, S., Robin, D. A., Fox, P. T. & Xiong, J. Changes occur in resting state network of motor system during 4 weeks of motor skill learning. *Neuroimage* **58**, 226-233, doi:10.1016/j.neuroimage.2011.06.014 (2011).

71 Deng, Z., Chandrasekaran, B., Wang, S. & Wong, P. C. Resting-state low-frequency fluctuations reflect individual differences in spoken language learning. *Cortex* **76**, 63-78, doi:10.1016/j.cortex.2015.11.020 (2016).

72 Bassett, D. S. & Mattar, M. G. A Network Neuroscience of Human Learning: Potential to Inform Quantitative Theories of Brain and Behavior. *Trends Cogn Sci* **21**, 250-264, doi:10.1016/j.tics.2017.01.010 (2017).

73 Heitger, M. H. *et al.* Motor learning-induced changes in functional brain connectivity as revealed by means of graph-theoretical network analysis. *Neuroimage* **61**, 633-650, doi:10.1016/j.neuroimage.2012.03.067 (2012).

Acknowledgments: We thank Prof. Yanchao, Bi, Prof. David Freedman, Prof. Huan Luo, Prof. Shan Yu, Dr. Matthew Rosen for their helpful comments on an earlier version of this manuscript. We also thank the veterinary staff at Peking University Animal Resources Center for expert assistance.

Funding:

Ministry of Science and Technology of the People's Republic of China, STI2030-Major Projects (2021ZD0203800), YZ;

National Natural Science Foundation of China, NSFC32171036, YZ.

Author contributions:

Conceptualization: YZ

Methodology: ZJ, ZL, LS, ST

Investigation: ZJ, ZL, LS, YZ

Visualization: ZL, ZJ, YZ

Funding acquisition: YZ

Project administration: YZ

Supervision: YZ

Writing – original draft: YZ

Writing – review & editing: FF, YZ

Competing interests: Authors declare that they have no competing interests.

Data and materials availability: All data and analyses necessary to understand and assess the conclusions of the manuscript are presented in the main text and in the supplementary materials.

Supplementary Materials

Figs. S1 to S12

Tables S1

Figures and Legends

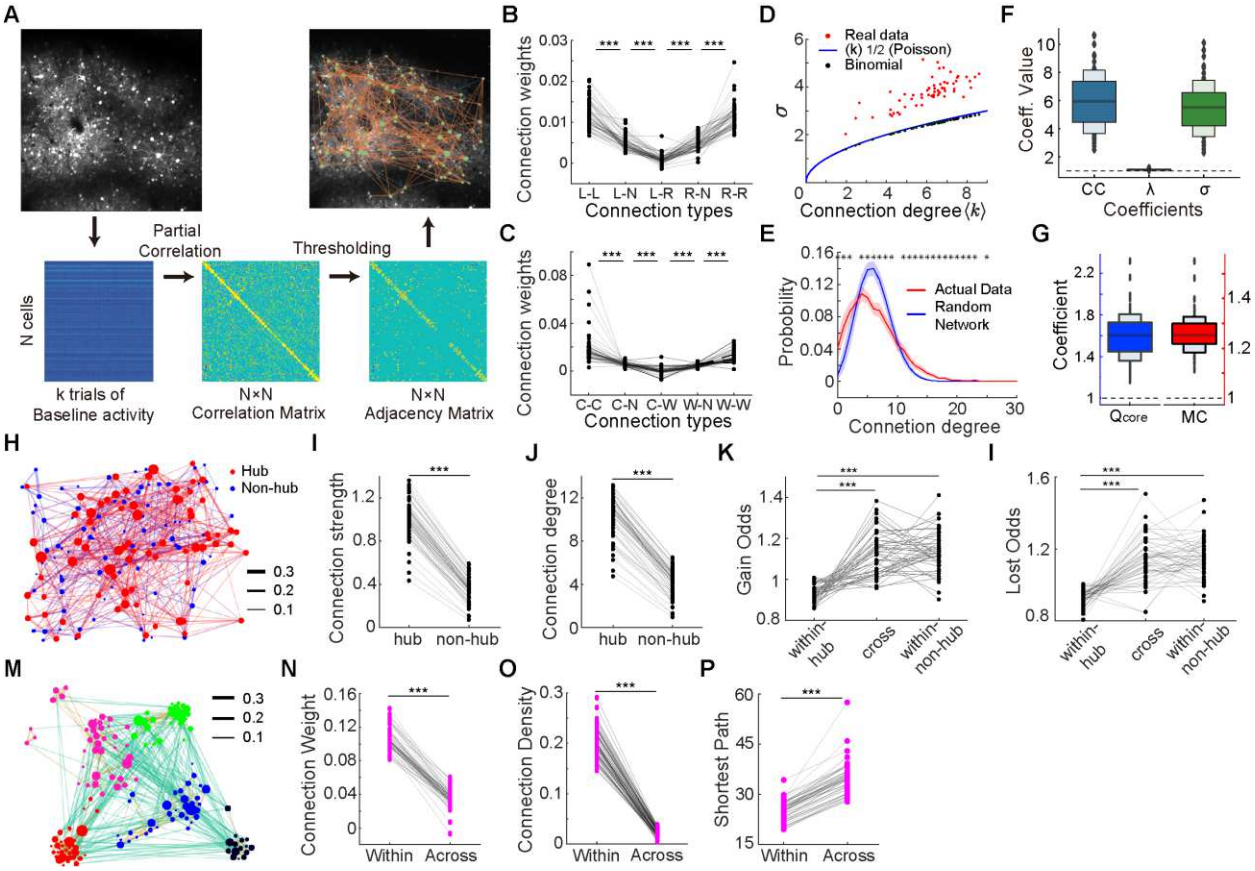


Fig. 1. The PPC neuron network exhibits small-world properties. **(A)** Procedure for constructing the neuron network. Partial correlations were calculated for each pair of simultaneously recorded neurons during a single recording session using activity from the fixation period of the Behavioral task. These correlations were used as connection weights to generate a connection matrix, with a threshold applied to exclude trivial connections. Green dots represent identified neurons of varying sizes. Brown and blue lines indicate positive and negative connection weights, respectively. **(B-C)** Comparisons of connection weights between neurons exhibiting the same or different saccade direction selectivity (B) or outcome selectivity (C). Each line connects the averaged results within one network. **(D)** Comparisons of the standard deviations of the connection degree between PPC neuron networks and random networks. Each dot represents the result of one network. **(E)** Distribution of connection degrees across all PPC networks, compared to random distributions with identical connection degree levels. **(F)** Clustering coefficient (CC), shortest path length (λ), and small-worldness (σ) of PPC networks relative to random networks. **(G)** Quality of hub/non-hub partitioning and modular organization across all networks, measured by the Qcore and modularity coefficient (MC) relative to ramdom networks (horizontal dashed lines). **(H)** Example network illustrating hub (red) and non-hub (blue) neurons distributed according to their spatial locations on the cortex. Dot sizes represent the connection degree of each neuron, while line widths indicate connection weights. **(I-J)** Comparisons of connection strength (I) and connection degree (J) between hub and non-hub neurons. Each dot denotes the averaged result of all hub/non-hub neuron in one network. **(K-L)** Comparisons of gain and loss odds of

connections among hub neurons, non-hub neurons, and hub–non-hub neuron pairs. **(M)** The module organization of the example network shown in (H), with different colors indicating distinct modules. Connections between and within modules were shown in brown and cyan, respectively. **(N-P)** Comparisons of connection weight (N), connection density (O), and shortest path length (P) between neurons within the same module versus those in different modules. ***: P << 0.001, **: P < 0.01.

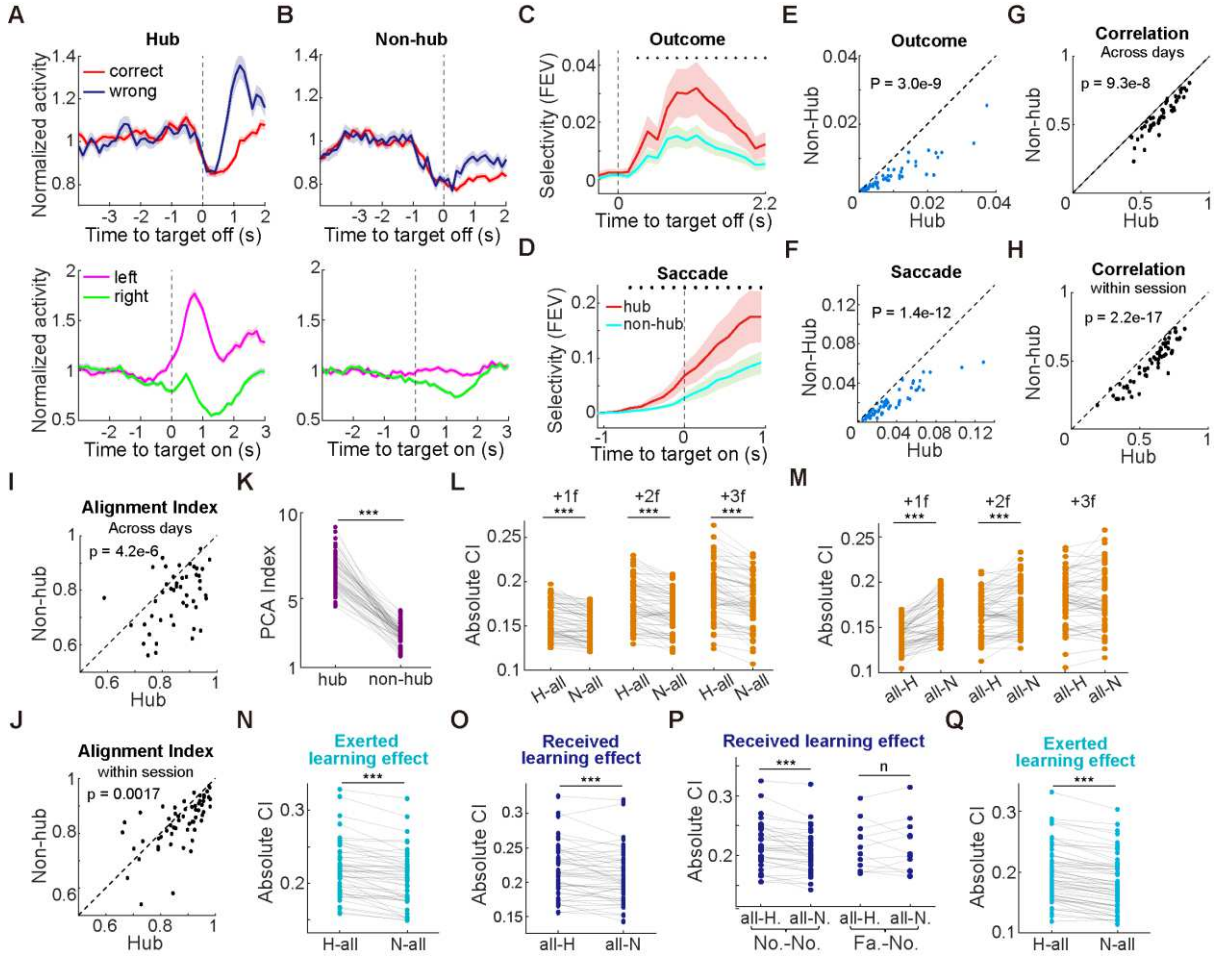


Fig. 2. Hub neuron plays a dominant role in both encoding key task variables and driving activity dynamics. A-F. Strength of neural encoding. **(A)** Two example hub neurons. The upper panel shows outcome selectivity, while the lower panel shows saccade direction selectivity. **(B)** Two example non-hub neurons. **(C-D)** Average strength of outcome selectivity (C) and saccade direction selectivity (D), quantified by the fraction of explained variance (FEV), shown separately for hub and non-hub neurons in an example network (* marks the time period during which there was a significant difference, p<0.01). **(E-F)** Comparisons of outcome selectivity (E) and saccade direction selectivity (F) between hub and non-hub neurons across all networks. **(G-J)** Stability of neural encoding. **(G-H)** Comparisons of the correlation of neural selectivity across two successive sessions (G) or within two halves of a single session (H) between hub and non-hub neurons. **(I-J)** Alignment index, quantifying the similarity of population neural activity, shown for two successive sessions (I) and within-session halves (J). **(K)** Comparisons of contribution to the

population activity dynamics between hub and non-hub neurons. The PCA index quantifies each neuron's contribution to the top 10 principle components of the population activity of each network. **(L)** A causality index (CI), which quantify the influence of each neuron's activity in the current time period to the activity of the other neurons in the later time periods in the same task trial, was compared between hub and non-hub neurons. Each dot denotes the averaged absolute value of the CI of all the hub/non-hub neurons in each network. **(M)** The CI was also used to quantify the influence of each neuron's activity in a given time period by the activity of the other neurons in the earlier time periods in the same task trial. **(N)** Comparisons of the received learning effect between hub and non-hub neurons. The CI was used for measuring the influence of each neuron's activity to the other neurons' selectivity to the key task variables in the following session (day). **(O)** Comparisons of the received learning effect between hub and non-hub neurons. The CI was used for measuring the influence of each neuron's selectivity to the key task variables by the activity of the other neurons in the earlier session (day). **(P)** Comparisons of the received learning effect, separating the situations in which the monkeys had been learning the same novel associations in the two successive days (No.-No.) or the monkeys transitioned from exploiting the learned associations to learn novel associations (Fa.-No.). **(Q)** Comparisons of the exerted learning effect. The CI was calculated using data in the earlier and later half of each recording session. H-all: hub neurons to all neurons; N-all: non-hub neurons to all neurons; all-H: all neurons to hub neurons; all-N: all neurons to non-hub neurons; No.-No.: from novel day to novel day; Fa.-No.: form familiar day to novel day.

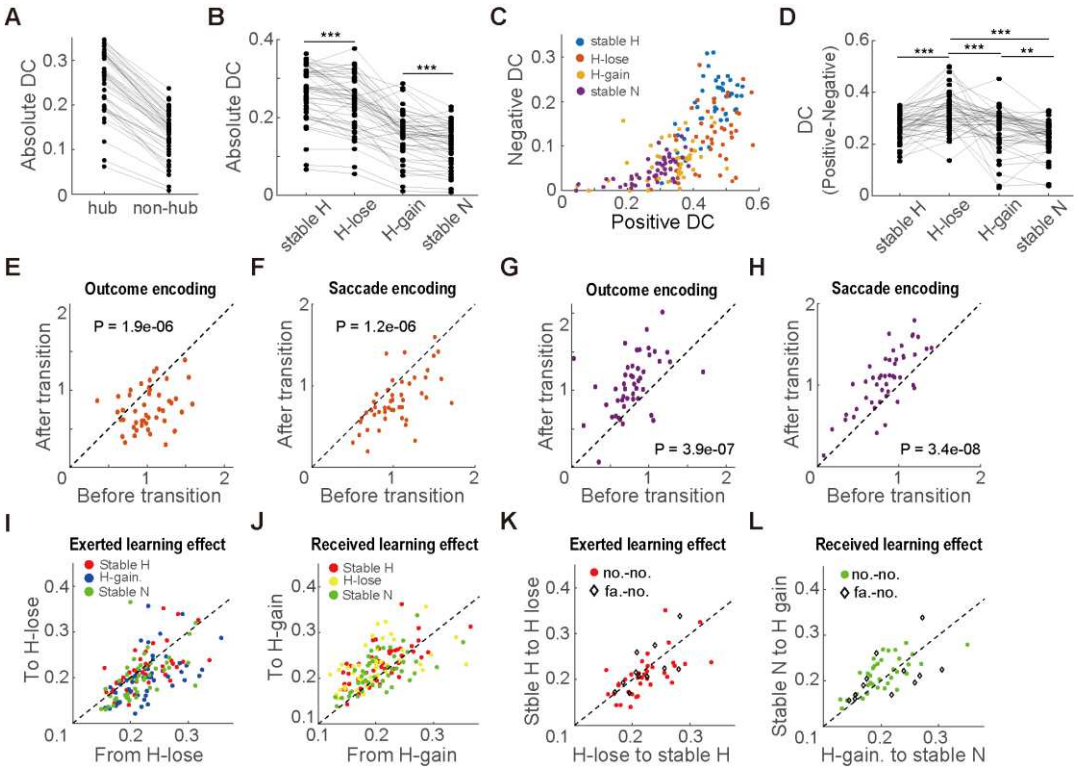


Fig. 3. Transitions in neurons' hub/non-hub status during learning. (A) Comparison of the global diversity coefficient (DC) between hub and non-hub neurons (both positive and negative DC). DC quantifies each neuron's inter-module connections relative to its within-module

connections. **(B)** Comparison of global DC between stable hub (stable H) neurons and hub-losing neurons (H-lose), as well as between hub-gaining (H-gain) neurons and stable non-hub neurons (stable N). **(C)** Separate plots of positive and negative DCs for stable hub neurons, hub-losing neurons, hub-gaining neurons, and stable non-hub neurons. **(D)** Comparison of the dominance of positive DC relative to negative DC among the four subsets of neurons. **(E-F)** Comparison of the encoding strength for trial outcome (E) and saccade direction (F) before and after the transition from hub to non-hub status in hub-losing neurons. **(G-H)** Comparison of the encoding strength for task variables before and after the transition from non-hub to hub status in hub-gaining neurons. **(I)** Comparison of the exerted learning effects between situations where hub-losing neurons influence other subsets of neurons versus situations where other subsets influence hub-losing neurons. **(J)** Comparison of the received learning effects between situations where hub-gaining neurons receive influence from other subsets versus situations where other subsets receive influence from hub-gaining neurons. **(K)** Comparison of the exerted learning effects between situations where hub-losing neurons influence stable hub neurons and where stable hub neurons influence hub-losing neurons. **(L)** Comparison of the received learning effects between situations where hub-gaining neurons receive influence from stable non-hub neurons and where stable non-hub neurons receive influence from hub-gaining neurons. In panels K and L, comparisons were made between situations where monkeys learned the same associations across two successive days versus when monkeys transitioned from exploiting learned associations to learning novel ones. H-lose: hub-losing neuron, H-gain: hub-gaining neuron.

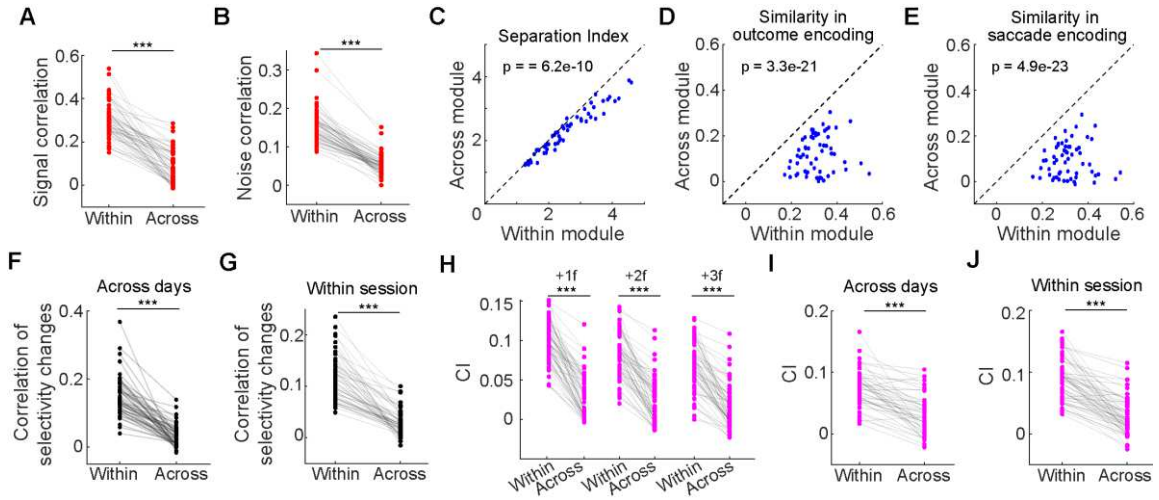


Fig. 4. Modular computation. (A-B) Comparison of signal correlation (A) and noise correlation (B) between neurons within the same module versus those in different modules. **(C)** Comparison of the separation index, which quantifies the separation of neural encoding for saccade direction and trial outcome, between neurons within the same module and those in different modules. A larger separation index indicates greater divergence in neural encoding between the two variables but smaller variations within each variable's encoding (see Method). **(D-E)** Comparison of similarity in neural encoding of trial outcome (D) and saccade direction (E). **(F-G)** Comparison of similarity (correlation) in neural selectivity changes across successive sessions (F) or across half sessions (G). **(H)** Comparison of mutual influence on activity dynamics between neurons in the within-module and across-module conditions, as reflected by the CI value. **(I-J)** Comparison of

mutual impact on the evolution of neural encoding during learning, measured by the CI, between within-module and across-module conditions. Data are shown separately for across days (I) and across half sessions (J).

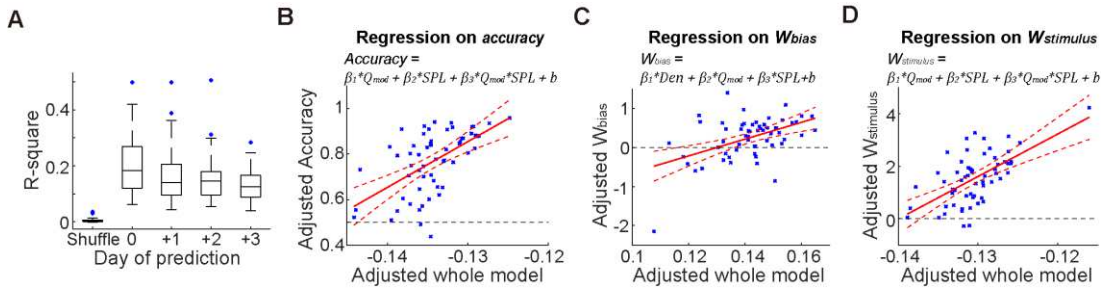


Fig. 5. Network properties predict neuron function similarity and monkeys' daily behavioral performance. (A) Small-world network properties significantly predict the similarity of neural encoding between neuron pairs within each PPC neuron network. A linear model incorporating four topological parameters predicted signal correlation not only within the same day but also across successive learning days. **(B-D)** Small-world network features also predict the monkeys' daily behavioral performance during learning. $W_{stimulus}$ and W_{bias} represent the extent to which the monkeys' saccade choice during each learning day was based on visual stimuli and internal bias, respectively. The short-path length (SPL), modularity (Q_{mod}) and their interaction were significant predictors of the monkeys' performance accuracy across learning days (B). The averaged connection density (Den), Q_{mod} and SPL were significant predictors of the monkeys' choice bias (C). The SPL, Q_{mod} and their interaction were also significant predictors of the monkeys' correct choices based on stimuli (D). Each dot represents one network. The red solid line indicates the linear fit, while the red dashed line represents the 95% confidence interval.

Supplementary Files

This is a list of supplementary files associated with this preprint. Click to download.

- SupplementarymaterialsPPCneuronnetwork.pdf